Energy 229 (2021) 120699

Contents lists available at ScienceDirect

Energy

journal homepage: www.elsevier.com/locate/energy

Online estimation of battery model parameters and state of health in electric and hybrid aircraft application

Seyed Reza Hashemi, Ajay Mohan Mahajan, Siamak Farhad*

Advanced Energy & Sensor Laboratory, Department of Mechanical Engineering, The University of Akron, Akron, OH, United States

ARTICLE INFO

Article history:
Received 30 October 2020
Received in revised form
8 April 2021
Accepted 16 April 2021
Available online 29 April 2021

Keywords:
Lithium-ion battery
Online parameter identification
Full electric aircraft
Hybrid electric aircraft
State of health
Battery management system

ABSTRACT

The accuracy of state of health (SOH) estimation function in battery management systems is an essential factor for ensuring the safety and reliability of battery systems in electric aircraft. Most common SOH estimation approaches are model-based and work with constant model parameters. However, the model parameters vary by the change in operating temperature and state of charge (SOC). The variation of model parameters has adverse impact on the accuracy of battery state's estimation if they are not updated. In this paper, an accurate online parameter estimation method is proposed for lithium-ion batteries (LIBs) to increase the accuracy of the battery model. A more accurate model for the battery leads to a more accurate SOC and SOH estimation. An adaptive sliding observer is developed to estimate the SOC and capacity based on the proposed parameter estimator. An adaptive SOH estimation scheme is proposed to mitigate the temperature variation effect on the accuracy of the SOH estimation. The experimental results verify the effectiveness of the proposed parameter estimator along with the adaptive sliding observer on achieving accurate estimation of SOC and capacity. The proposed adaptive SOH shows good agreement with experiments by less than 1.3% estimation error at different operating temperature conditions.

1. Introduction

Recently, research on electrifying aircraft has attracted more attention like it has on electric vehicles. In these devices, the role of electrical power systems has grown from simple functions to relatively critical ones such as propulsion system for couple of reasons [1]. Higher flight efficiency and more sustainable energy source are major reasons for these changes. Lately, high-power density batteries and highly efficient electrical motors have been developed by researchers [2,3]. By these successes, heavy mechanical components in aircraft such as combustion system can be replaced by electrical components toward improving flight efficiency and weight reduction [4]. Because of similarities and common points between electric vehicles and electric aircraft, the improvement in one can lead to the improvement of the other. However, their differences must also be considered in their design stages. In both electric vehicle (EV) and electric aircraft (EA) or hybrid electric vehicle (HEV) and hybrid electric aircraft (HEA), the same energy storage methods can be used. Meanwhile, due to different aerodynamic features, the characteristics of electrical loads are somewhat different in these two applications. Since the regenerated energy in EA is relative to its flight speed, the power dynamic in aeronautic domain is sharp in comparison with the one in EV [5,6]. Therefore, the choice of quality, size and type of energy is influenced by these various features.

Lithium-ion batteries (LIBs) have become prominent energy-storage devices for electrified vehicles/aircraft due to their high energy density and long life. In these applications, LIBs are monitored and controlled by a battery management system (BMS) [7,8]. BMS has different responsibilities including estimation of state of charge (SOC), fault diagnosis, estimation of state of health (SOH), thermal management, cell balancing of the batteries, etc. [9]. The performance and accuracy of these functions in BMS is highly dependent on the accuracy of the model developed for the LIBs [10]. SOH is an energy indicator for a cell which shows the ability difference of storing and releasing energy in the cell between its current and initial condition [11,12]. Usually, when SOH has fallen to 80%, the battery needs to be replaced before the EA/HEA crashes due to the battery failure [13]. The calculation of SOH is generally based on either the capacity reduction or the internal resistance

* Corresponding author.
E-mail address: sfarhad@uakron.edu (S. Farhad).

https://doi.org/10.1016/j.energy.2021.120699
0360-5442/

increments in batteries [14]. The resistance-based approaches are insensitive to discharge level and effective in estimating the remaining capacity of the cell. However, due to its time-consuming process, these approaches are more suitable for stationery or offline applications [15]. Therefore, a capacity-based SOH estimation approach is proposed in this study which is based on the ratio of the cell's maximum capacity to its nominal capacity.

A standard capacity test (SCT) is the most practical method to obtain the battery capacity and SOH by discharging the battery from the full charge level to the cut-off voltage of discharge [16]. However, it is difficult to implement SCT on battery cells in EA/HEA to measure their capacities. As a result, estimating capacity and SOH accurately is essential but challenging in BMS. So far, various researches on the SOH estimation have been investigated. Typically, estimation approaches are categorized into data-driven and model-based methods. In the data-driven category, some methods like machine learning and neural networks have an assigned memory and a proper nonlinear function for estimation [17–19]. In this category, to have a good overall performance and accurate estimation, mostly heavy calculations and computational time are required [20]. In addition, this category needs a large number of tests and experimental datasets such as temperature, SOC, voltage and current [21]. Thus, in the data-driven approaches, pre-processing data and minimizing noise are critical. In the second category which is model-based, some measured parameters such as current, temperature, terminal voltage are utilized as the inputs of the battery model to estimate SOH [22–24]. During battery operations, the model-based SOH estimation methods proved to have more efficiency and greater robustness in compared with the data-driven ones [25,26]. However, the accuracy of estimation and the level of robustness depends on the battery model accuracy. Equivalent circuit models (ECMs) and electro-chemical models are mostly used by researchers for dynamic modeling of LIBs [27]. The electro-chemical ones are not feasible in the BMS applications, because of their partial differential equations which need too much memory and computational time [28]. Some common model-based SOH estimation methods such as extended Kalman filters (EKFs) [29], recursive least square (RLS) [30], and particle filter (PF) have been used frequently by researchers [31]. However, in these methods, ignoring the impact of battery aging and operating temperature on the accuracy of battery model can lead to an inaccurate SOH estimation.

The simplicity and robustness of ECMs make them reliable options for real-time applications in BMS. ECM of a battery may contain capacitances, resistances, and an open voltage source to represent the cell behavior. ECMs typically come with one, two or three resistance-capacitance (R–C) networks. The second order ECM is proved to simulate the dynamic behavior of battery accurately with low computational time [32]. Higher order ECMs with more than two R–C networks cause higher computational effort without dramatically increasing the accuracy of the battery model [33,34]. Moreover, along with the second order battery model, an accurate parameter identifier is a key factor for improving the accuracy of the model and SOH estimation. Among different offline identification techniques, Hybrid Pulse Power Characterization (HPPC) [35] and Electrochemical Impedance Spectroscopy (EIS) [36] are frequently used for the ECM parameter characterization tests. Experiments have shown in different SOCs, temperatures and load levels, the value of battery parameters vary [37,38]. Thus, considering constant values for these parameters leads to an inaccurate ECM [39,40]. Consequently, by an inaccurate ECM, the accuracy of some model-based functions of BMS such as SOC and SOH estimation would be negatively affected. Therefore, an online parameter estimator is required for the battery model to improve the BMS performance [41]. used EKF for identification of time-variant ECM parameters. Some other methods such as weighted RLS (WRLS) and adaptive filters were applied for online parameter identification by different researchers [42–44]. In this paper, an online parameter estimator based on an exponential regression algorithm (ERA) is proposed for identification of the ECM parameters. Using this online parameter estimator, the negative impact of some elements such as temperature and aging on the accuracy of ECM can be mitigated. Moreover, we have developed an adaptive sliding mode observer based on the proposed adaptive ECM for the SOC estimation. At the final stage, an adaptive estimation scheme is proposed to mitigate the temperature effect on the accuracy of the SOH estimation in the battery. The main contributions of this paper include:

- We proposed an online parameter estimator using an exponential regression algorithm to form an adaptive ECM (AECM).
- Based on the proposed AECM, we developed an adaptive slide mode observer for the SOC and capacity estimation.
- Validation tests displayed high accuracy of the proposed AECM and SOC estimator with Mean Absolute Error (MAE) of 0.0015 and Root mean squared error (RMSE) of 0.0006 in the SOC estimations.
- We proposed an adaptive SOH estimation scheme to calculate the battery SOH accurately by mitigating the negative impact of operating temperature variation.
- To complete the proposed SOH estimation scheme, besides calculating the battery capacity online, we calculated the capacity of a fresh battery in different temperatures and formed a capacity-temperature lookup table using experiments.
- Using experimental tests, the accuracy of the proposed adaptive SOH scheme was validated at the final stage.

The arrangement of this study is as following: Section 2 discusses the battery test setup and experiment approach conducted in this study. Section 3 illustrates the battery modeling development procedure and the proposed parameter estimator. Section 4 presents the strategy of developing an adaptive SOC and capacity estimation technique. Section 5 talks about the proposed adaptive SOH scheme. In Section 6, the proposed adaptive estimation approaches for model parameters, SOC and SOH are validated and discussed in different experiment conditions.

2. Battery setup and experiments

In this study, a battery cycler is used to conduct cycling tests on cells under different dynamic charging-discharging profiles. The charging and discharging process is controlled using a LabVIEW program on a computer. An accurate data logger is added to the setup to collect battery data and store them in the computer. In addition, the temperature of the cells' condition is controlled and monitored inside of a chamber.

2.1. Experiment bench

In order to develop the proposed SOH estimation scheme and validate its accuracy, the experiment setup shown in Fig. 1 is established. The experiment setup and experiment approach of this study is intended to be applied for designing and developing battery management systems in EAs. The main components of this experiment bench incorporate a data collector, temperature chamber, computer, and battery cycler as listed in Table 1. In this work, LTO-1020 which is a type of LIBs is used as the energy source of EA/HEA applications due to its advantages of fast charging and longer life than other types of LIBs [45,46]. This LIB specifications

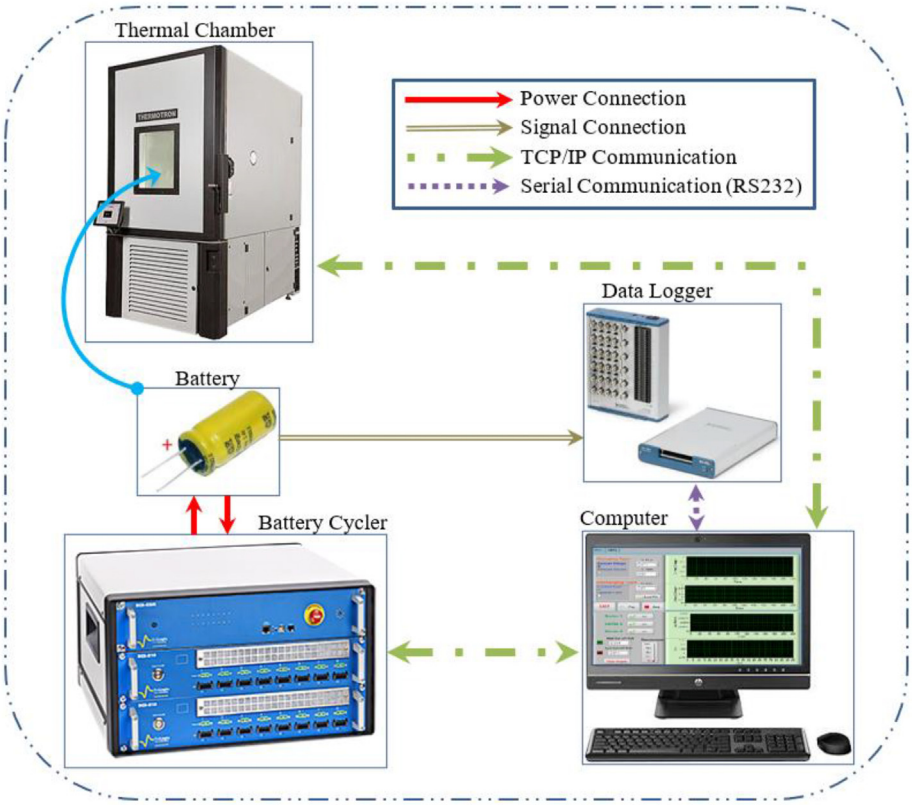

Fig. 1. Experiment setup for battery.

Table 1
Experiment components.

#	Part	Model
1	Data Collector	NI: USB-6343
2	Temperature Chamber	SE-2000
3	Host Computer	Dell 790, Intel Core i7, 16 GB RAM, 512 GB SSD
4	Battery Cycler	BioLogic: BCS-810
5	Battery Cell	LTO-1020

includes nominal voltage of 2.4 V, nominal rated capacity of 50 mAh, maximum charging rate of 20 °C, maximum discharging rate of 40 °C and operating temperature range between −20 °C and 60 °C.

Here, for charging and discharging the batteries, a BioLogic cycler is used. This battery cycler has an 18-bit current/voltage resolution, and it delivers 8 independent channels with current and voltage ranges of ±1500 mA and 0–10 V, respectively. The temperature of operation for the experiments can be controlled in the range of −70 °C–180 °C with the accuracy of ±0.3°C using the temperature chamber (SE-2000).

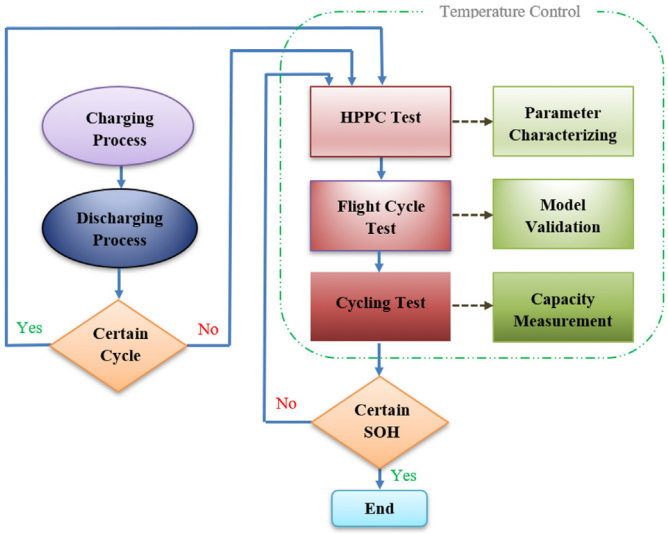

Fig. 2. Battery experiment approach.

2.2. Experiment approach

The experiment approach is designed and developed based on two main stages as shown in Fig. 2: A) a cycling/aging part in which LIBs are cycled based on predefined charging-discharging profiles and number of cycles; B) a characterization part which has the responsibility of parameters' identification of the LIBs under cycling processes. The cycling part is carried out to analyze the battery's aging process and evaluate the proposed SOH estimation scheme. After some predefined cycles, the characterization part is conducted periodically to identify the LIB parameters in different temperatures along with aging process. The operating temperature of these experiments is controlled in the thermal chamber. In this study, the temperature range was from 10 °C to 40 °C, because the operating temperature does not exceed this range in the battery system of EA. Moreover, during the experiments, the dataset is built by recording voltage, current and operating temperature with the sampling rate of 0.01 s.

The experiments of characterization part include HPPC test,

flight cycle test and cycling test by which ECM parameter identification, model validation and capacity calculation are carried out, respectively. In HPPC tests, a current profile that includes both charge and discharge pulses are applied to characterize the dynamic properties of a battery [47]. For characterization process, under a controlled condition, the voltage and current of the battery are monitored. In this study, the charging/discharging profile contains discharge pulses of 50 mA, 100 mA and 150 mA and charge pulses of 25 mA, 50 mA and 75 mA. Moreover, the cell under HPPC tests starts with SOC of 90% to reach10% with an interval of 10% SOC and a rest time of 2 h. Moreover, for flight cycle tests, a set of real flight profiles were adopted based on overall specifications of EA regardless of their sizes or capabilities. These profiles are defined in terms of the characteristics of energy demand in EA. Plus, to determine specific performance of battery cells, flight profiles can be utilized in different combinations with convenient scaling factors. Finally, SCT tests are carried out to obtain the capacity and SOH of the battery by discharging the battery from the full charge level to the cut-off voltage of discharge.

In the stage of validation experiments, LTO1020 cells were tested under a real flight profile with low C-rates to simulate an actual flight cycle. This flight cycle profile contains speed information for emission testing of aircraft. And in the second stage, LTO battery cells were tested under a high C-rate flight cycle. Flight cycle profiles were generated with a convenient scaling factor related to the cells' specifications in an EA simulator that we developed in LabVIEW. In both stages, the temperature set-point can be entered before test (10 °C–40 °C). The data collected from the experiments is applied to evaluate the performance of the proposed SOC and SOH estimators over the battery aging.

3. Battery modeling and parameter estimation

Developing an accurate battery model leads to improve the BMS performance since most of its functions such as fault diagnosis, cell equalization, SOC and SOH estimations are model based. In addition, an improved BMS system leads to having a better performance in the battery cells and maximizing their lifespan.

3.1. Battery modeling

ECMs are frequently applied for LIBs to simulate their behavior. Among different ECMs, Dual Polarization (DP) model shown in Fig. 3 has proved to be accurate for the BMS application [48,49]. This ECM contains an ohmic resistance, two pair of resistance-capacitor network and the Open Circuit Voltage (OCV). Using these components and the following equations, ECM model can be formed to simulate the dynamic behavior of LIB:

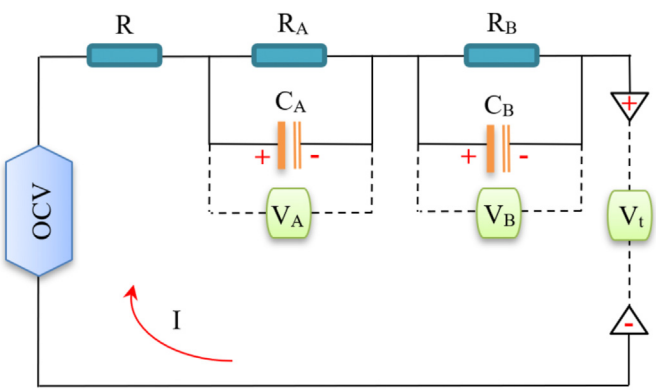

Fig. 3. Second order ECM for the LIB.

$$V_t = OCV - IR - V_A - V_B \tag{1}$$

$$\dot{V}_A = -\frac{1}{C_A R_A} V_A + \frac{1}{C_A} I \tag{2}$$

$$\dot{V}_B = -\frac{1}{C_B R_B} V_B + \frac{1}{C_B} I \tag{3}$$

which can be rewritten in the discrete format as shown:

$$V_t(k) = OCV - IR - V_A(k) - V_B(k) \tag{4}$$

$$V_A(k+1) = V_A(k) e^{-\frac{T_s}{\tau_A}} + I_k R_A \left(1 - e^{-\frac{T_s}{\tau_A}}\right) \tag{5}$$

$$V_B(k+1) = V_B(k) e^{-\frac{T_s}{\tau_B}} + I_k R_B \left(1 - e^{-\frac{T_s}{\tau_B}}\right) \tag{6}$$

where, τ represents the time constant of the R–C networks which is equal to $R \times C$. The sample sequence is shown by k, and the sample time which is 0.01 s is denoted by T_s.

3.2. Online battery parameter identification

The variation in the values of ECM parameters at different temperature conditions is critical for the accuracy of a developed LIB model [50]. Since the estimation accuracy of SOC and capacity depends on the accuracy of ECM, having a reliable identification approach for ECM parameters is essential. Some researchers used lookup tables to minimize the dependency of ECM parameters on the operating temperature [51]. However, they don't consider the impact of the cell aging on the ECM parameters in their lookup tables. Therefore, an online ECM parameter estimator can be a good solution to this problem. In this study, in order to improve the SOH estimation of LIB, an exponential regression algorithm (Fig. 4) is exploited to develop an online parameter estimation method for ECM.

To identify the battery model parameters, a technique described by Schweighofer [52] has been applied. In this technique, to characterize the LIBs, a programmable resistive load is connected to the pack temporally using a trigger command. By observing the current changes from one discrete value to another, the bulk resistance (R) of ECM can be calculated using Eq. (7).

$$R = \frac{V_p - V_a}{\Delta I} \tag{7}$$

where, ΔI represent the current changes, V_p and V_a are the terminal voltage prior to the current changes and the terminal voltage right after the load changes, respectively. After finding the R value, the transient behavior of the cell in the interval from the moment the current level changes (t_0) to the moment in which the terminal voltage becomes constant can be used to find R_A, C_A, R_B and C_B. In this process, the temperature, current and terminal voltage of the cells are collected. By rewriting Eq. (4), the terminal voltage during this interval can be described by Eq. (8).

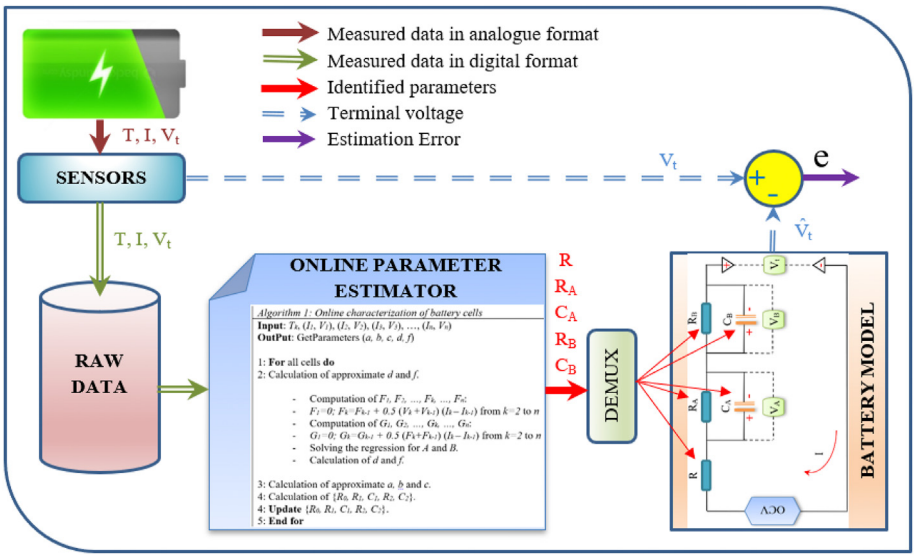

Fig. 4. The proposed online ECM parameter estimation method.

$$\begin{pmatrix} A \\ B \\ C \\ D \\ E \end{pmatrix} = \begin{pmatrix} \sum G_k^2 & \sum G_k F_k & \sum G_k I_k^2 & \sum G_k I_k & \sum G_k \\ \sum G_k F_k & \sum F_k{}^2 & \sum F_k I_k^2 & \sum F_k I_k & \sum F_k \\ \sum G_k I_k^2 & \sum F_k I_k^2 & \sum I_k^4 & \sum I_k^3 & \sum I_k^2 \\ \sum G_k I_k & \sum F_k I_k & \sum I_k^3 & \sum I_k^2 & \sum I_k \\ \sum G_k & \sum F_k & \sum I_k^2 & \sum I_k & n \end{pmatrix}^{-1} \begin{pmatrix} \sum G_k V_k \\ \sum F_k V_k \\ \sum I_k^2 V_k \\ \sum I_k V_k \\ \sum V_k \end{pmatrix} \tag{12}$$

$$V_t(t) = OCV(t_0) - V_A(t_0)\cdot\exp(-t/R_A C_A) - V_B(t_0)\cdot\exp(-t/R_B C_B) - R\cdot I_a \tag{8}$$

At time t_0, $V_A(k+1) \approx V_A(k)$ and $V_B(k+1) \approx V_B(k)$, then Eqs. (5) and (6) can be written to the following form:

$$V_A(k) = R_A \cdot I(k) \tag{9}$$

$$V_B(k) = R_B \cdot I(k) \tag{10}$$

Eq. (11) contains two exponential terms which represent the transient periods corresponding to the two R–C networks in ECM. As illustrated in Table 2, the ECM parameters can be characterized through a curve fitting method and by the following generic equation with two exponential terms and five parameters (a, b, c, d and f) [51].

$$V(I) = a + b\cdot e^{dI} + c\cdot e^{fI} \tag{11}$$

As shown below, the five parameters d, f, a, b and c regression involve a 5×5 matrix. In the first step, to fit Eq. (11), the measured terminal voltage V_k and current I_k are applied to solve the regression system for A and B in Eq. (12). Then, A and B values are applied to calculate d and f by Eq. (13).

$$Approximation: \begin{cases} d \approx 0.5\left(B + \sqrt{B^2 + 4A}\right) \\ f \approx 0.5\left(B - \sqrt{B^2 + 4A}\right) \end{cases} \tag{13}$$

In the second step, the calculated d and f from the first step are

Table 2
ECM parameter estimation by an exponential regression algorithm.

Algorithm: Online characterization of battery cells
Input: T_k, (I_1, V_1), (I_2, V_2), (I_3, V_3), …, (I_n, V_n)
OutPut: GetParameters (a, b, c, d, f)
1: **For** all cells **do**
2: Calculation of approximate d and f.
- Computation of F_1, F_2, …, F_k, …, F_n:
- $F_1 = 0$; $F_k = F_{k-1} + 0.5\,(V_k + V_{k-1})\,(I_k - I_{k-1})$ from k = 2 to n
- Computation of G_1, G_2, …, G_k, …, G_n:
- $G_1 = 0$; $G_k = G_{k-1} + 0.5\,(F_k + F_{k-1})\,(I_k - I_{k-1})$ from k = 2 to n
- Solving the regression for A and B.
- Calculation of d and f.
3: Calculation of approximate a, b and c.
4: Calculation of {R, R_A, C_A, R_B, C_B}.
5: **Update** {R, R_A, C_A, R_B, C_B}.
End for

applied to calculate a, b and c from Eq. (14).

$$\begin{pmatrix} a \\ b \\ c \end{pmatrix} = \begin{pmatrix} n & \sum e^{dI_k} & \sum e^{fI_k} \\ \sum e^{dI_k} & \sum e^{2dI_k} & \sum e^{(d+f)I_k} \\ \sum e^{fI_k} & \sum e^{(d+f)I_k} & \sum e^{2fI_k} \end{pmatrix}^{-1} \begin{pmatrix} \sum V_k \\ \sum V_k e^{dI_k} \\ \sum V_k e^{fI_k} \end{pmatrix} \tag{14}$$

Then, the parameters of the cell model can be obtained from Eq. (15) as

$$R = a, \quad R_A = -\frac{b}{I}, \quad C_A = -\frac{1}{R_A c}, \quad R_B = -\frac{d}{I}, \quad C_B = -\frac{1}{R_B f}. \tag{15}$$

After developing the ECM parameter estimator, the battery model is complete and can be used for different functions in BMS such as SOC and SOH estimations.

4. Adaptive SOC estimation method

The definition of SOC is the ratio of the current capacity of battery to its maximum capacity. In the previous sections, the battery model and the proposed parameter estimator were illustrated in detail. Here, the built AECM along with an adaptive sliding-mode observer are utilized for SOC estimation of the cell as shown in Fig. 5.

As depicted in Fig. 5, the SOC estimation process includes several steps: 1) Measurement of current and voltage by accurate sensors and initialization of necessary parameters; 2) Identification of the battery model parameters and updating them in ECM; 3) Implementation of the adaptive sliding mode observer on the parameters obtained from previous steps; 4) Estimation of SOC by mapping the calculated OCV.

To design the SOC estimation scheme, ECM needs to be transformed to a discrete time model. Eq. (2) is rewritten using the first-order forward Euler method and the measured terminal voltage as following [53]:

$$V_t(k+1) = \left(1 - \frac{T_k}{\tau_A} - \frac{T_k}{\tau_B}\right)V_t(k) + \left(\frac{T_k}{\tau_A} + \frac{T_k}{\tau_B}\right)OCV(k) - \left(\frac{T_k}{C_n} + \frac{T_k}{C_A} + \frac{T_k}{C_B} + \frac{T_k \cdot (R_A\tau_B + R_B\tau_A)}{\tau_A\tau_B}\right)I(k) \tag{16}$$

And the adaptive sliding-mode observer will be:

$$\tilde{V}_t(k+1) = \left(1 - \frac{T_k}{\tau_A} - \frac{T_k}{\tau_B}\right)\tilde{V}_t(k) + \left(\frac{T_k}{\tau_A} + \frac{T_k}{\tau_B}\right)JV_{sc} - \left(\frac{T_k}{C_n} + \frac{T_k}{C_A} + \frac{T_k}{C_B} + \frac{T_k \cdot (R_A\tau_B + R_B\tau_A)}{\tau_A\tau_B}\right)I(k) \tag{17}$$

$$\varepsilon(k+1) = \left(1 - \frac{T_k}{\tau_A} - \frac{T_k}{\tau_B}\right)\varepsilon(k) + \left(\frac{T_k}{\tau_A} + \frac{T_k}{\tau_B}\right)OCV - \left(\frac{T_k}{\tau_A} + \frac{T_k}{\tau_B}\right)JV_{sc} \tag{18}$$

Here, J represents the sliding-mode observer gain of V_{SC} which is the switching control vector; T_k is the observer sampling period. The ECM parameters obtained from the proposed online parameter estimator are updated in Eq. (17). By subtracting Eq. (16) from Eq. (17), ε(k) is obtained which represent the voltage estimation error. Then, the dynamic of the adaptive sliding-mode observer can be shown by Eq. (19) since ss(k) = ε(k) = 0. ss(k) represent the sliding surface.

$$\frac{ss(k+1) - ss(k)}{T_k} = \left(\frac{1}{\tau_A} + \frac{1}{\tau_B}\right)(-ss(k) + OCV(k) - JV_{sc}) \tag{19}$$

For the adaptive sliding-mode observer, the variable switching function is set as below:

$$V_{sc} = \begin{cases} V_{SC0} & \varepsilon(k) > V_{SC0} \\ \varepsilon(k) & -V_{SC0} > \varepsilon(k) > V_{SC0} \\ -V_{SC0} & \varepsilon(k) > V_{SC0} \end{cases} \tag{20}$$

Here, V_{SC0} represents the boundary layer width. Moreover, the stability condition of Lyapunov is met if $J > OCV_{max}/V_{SC0}$. The selector module will discard highly oscillated values and the moving average will smooth JV_{SC0}. As shown in Fig. 6, the estimated OCV is utilized for the SOC calculation based on the OCV-SOC relation. To reduce the SOC calculation error, a closed loop coulombic counting algorithm is cooperating with the established adaptive sliding-mode observer as follows [53]:

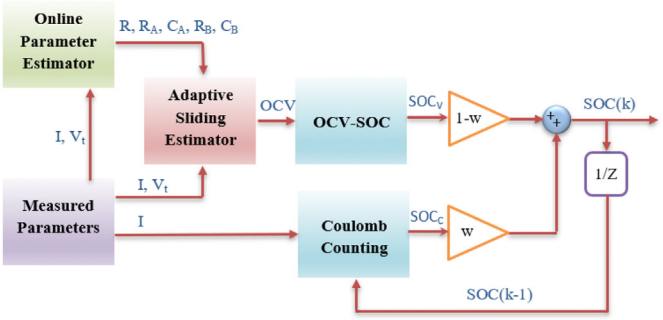

Fig. 6. The developed closed loop weighting SOC estimation algorithm.

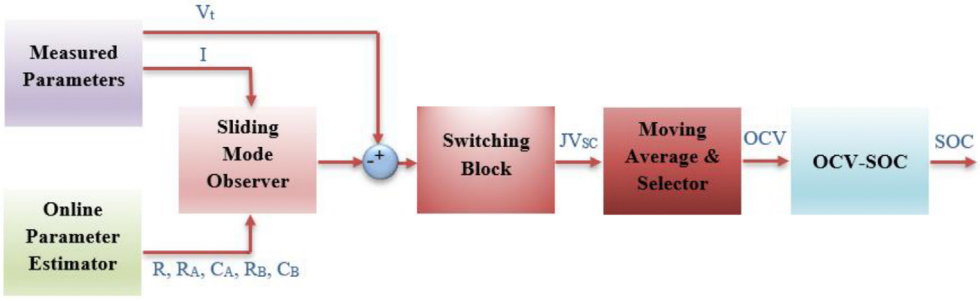

Fig. 5. The block diagram of the adaptive sliding SOC estimator.

$$SOC(k) = w.SOC_C(k) + (1-w).SOC_V(k) \tag{21}$$

$$SOC_C(k) = SOC(k-1) - \frac{1}{C_k}[I(k-1)\cdot T + \Delta C_U(k-1)] \tag{22}$$

where, w denotes the weighting factor which is from 0 to 1; C_k represents the battery estimated capacity; the SOC estimated by the adaptive slide mode observer is denoted by SOC_V. The estimated SOC (SOC_V) will be utilized in the SOC compensator to correct SOC_C. The SOC compensator efficiency is highly dependent upon the accuracy of the identified ECM parameters and the weighting factor. If the closed coulombic counting is only used for SOC estimation, the default value of weighting factor w will be one.

5. Online capacity and SOH estimation

In this section, the Capacity calculation approach and proposed adaptive SOH estimation method are illustrated. SOH is an index which represents the general state and capacity of the cell compared with a new fresh cell in producing the specified energy.

5.1. Online capacity estimation

The actual capacity of battery is not usually equal to its nominal capacity provided by the manufacturer because of the battery state variations. One of the reasons that causes these variations is the temperature changes. In addition, a cell 's maximum capacity can diminish because of ageing. Thus, the battery capacity of the cell (C_k) which is a proper indicator for the SOH estimation can be obtained using the SOC estimated from Eq. (21).

$$C_k(i) = \frac{T\sum_{i=k-1}^{k} I(i) + C_U(i)}{SOC(k-1) - SOC(k)} \tag{23}$$

where, k-1 and k correspond to the start and end time of the capacity estimation interval. Then, the SOH or capacity degradation of the battery is calculated by Eq. (24) in which the maximum current capacity (C_k) divided by the maximum capacity when the battery is fresh (C_n).

$$SOH(i) = \frac{C_k(i)}{C_n(i)} \times 100\% \tag{24}$$

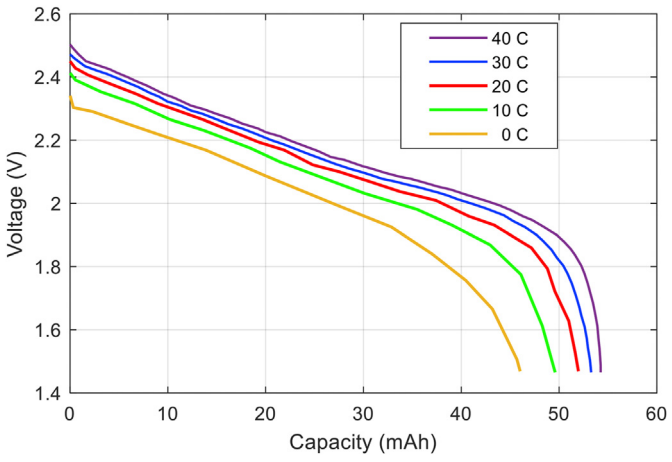

Fig. 7. Discharge voltage of LTO1020 cell at various temperatures (the unit of temperatures is degree Celsius).

As discussed, the cell capacity changes by the temperature variation. In order to increase the accuracy of SOH calculation, C_n of the cell can be updated based on the temperature of the interval in which the maximum current capacity of the battery is estimated. Therefore, we prepared a capacity-temperature look-up table by various experiments on a fresh cell in different operating temperatures. The voltage-capacity plots of these experiments are shown in Fig. 7.

5.2. Online SOH estimation

The battery health status can be indicated quantitatively by SOH which shows the ratio of the current performance of the battery to its nominal performance after a period that battery is used or cycled. However, there is no uniform definition for SOH. Here, the ratio of the cell capacity at the current moment to its nominal capacity (fresh) is applied for the SOH calculation. The framework of the online SOH algorithm which is proposed in this study can be seen in Fig. 8.

As shown in Fig. 8, the capacity of the battery in a current cycle and its capacity when it was fresh (first cycle) in the same temperature will be calculated. The current capacity of the cell is calculated by what discussed in Section 5.1. On the other hand, the battery capacity in its fresh status is estimated using a predefined capacity-temperature lookup table which is based on the current operating temperature. Then, SOH is calculated online by Eq. (24) using the estimated C_k and C_n.

We used the estimated data and the measured set to assess the generalization and robustness of the proposed SOH model. The mean absolute error (MAE) and root mean square error (RMSE) of data are calculated by Eqs. (25) and (26) as the evaluation criterion in this study.

$$MAE = {}^{100}/_{n}\sum_{i=1}^{n}\left|SOH_i - \widehat{SOH}_i\right| \tag{25}$$

$$RMSE = \sqrt{\frac{\sum_{i=1}^{n}\left(SOH_i - \widehat{SOH}_i\right)^2}{n}} \tag{26}$$

6. Results and discussion

In this work, the battery model is developed based on the proposed parameter estimator. Then, numerous experiments are conducted to verify the proposed estimation approaches for ECM parameters and SOH. The required data of the battery cells such as current, voltage and temperature are measured and recorded using the bench test described in Section 2.

6.1. Online parameter estimation results

This section presents the experiment results of the proposed ECM parameter estimator and compare them with the HPPC test results. At first, the cell is charged to 100% by CC-CV approach. Then the battery is simulated under an airway flight scenario using the flight cycle profile shown in Fig. 9 until the cell reaches its cut-off voltage. This flight cycle for HEA includes both discharge and charge profiles. The discharge process occurs in the takeoff and climb phases of HEA flight when electric motors along with combustion turbine(s) are involved in the propulsion system of the HEA. The charging process happens during the cruise and descent phases when the turbine(s) can be used to drive electric generators

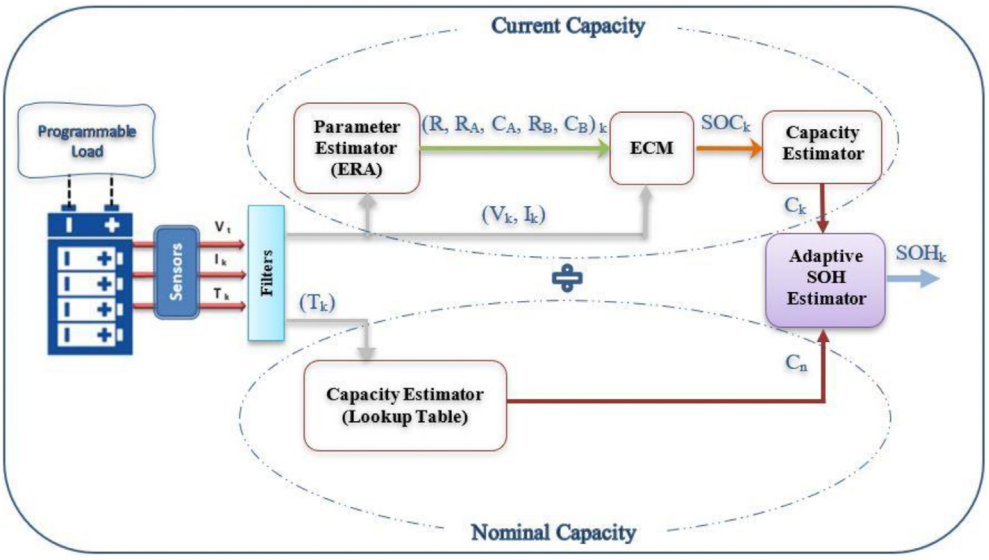

Fig. 8. The proposed online SOH estimation method.

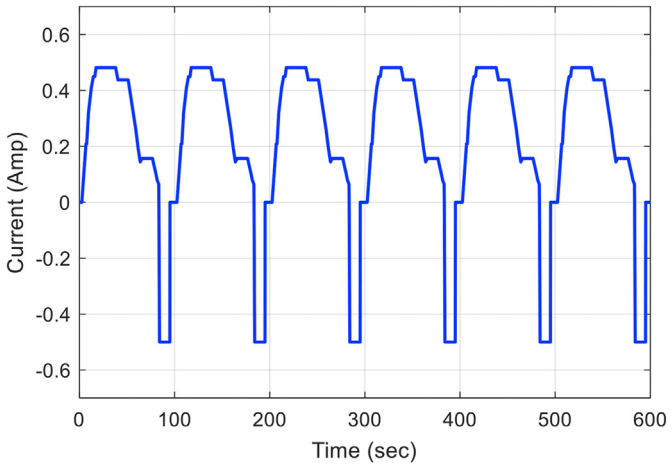

Fig. 9. A sequence of 6 cycles, separated by charge pulses.

to recharge batteries.

Fig. 10 shows the results of the ECM parameters estimated by the proposed algorithm under the flight cycle test. It should be noticed that the real values of the ECM parameters are identified by the HPPC experiments. As shown in Fig. 10, the proposed parameter estimator results have a good agreement with the real parameter values gained by HPPC. Using this parameter estimator and under the same flight cycle, the battery model performance at 25 °C can be obtained, as shown in Fig. 11. To see the effectiveness of the proposed parameter estimator on the accuracy of the battery model, the MAE and RMSE of voltage errors are calculated in different experiments. The MAE of 0.0571 and RMSE of 0.0022 in various flight cycles verify the accuracy of the battery model, and consequently the accuracy of the proposed parameter estimator.

6.2. Adaptive SOC estimation results

This section illustrate a comparative investigation of the adaptive SOC estimation results that we developed in this study. As the first case study, the flight cycle profile shown in Fig. 9 is applied for validation of the developed SOC and capacity estimation method. Moreover, Coulomb counting method along with a high accurate current sensor are used for the calculation of true SOC. The SOC and capacity estimation results of the first case study are compared with the experimenal results as plotted in Fig. 12.

In the second case study for the verification of the developed adaptive SOC and capacity scheme, the flight cycle shown in Fig. 13 is used. This flight cycle profile includes several flight cycles with low C-rates. The SOC and capacity estimation results of the second case study are compared with the experimenal results as depicted in Fig. 14.

The SOC and capacity estimation results presented in this section demonstrate that the developed adaptive SOC estimatation scheme have good match with the experiments. In addition, MAE and RMSE are applied to calculate the difference between the estimated SOC values and the real SOC values. The calculated MAE and RMSE from the SOC validation test results are 0.0015 and 0.0006, respectively.

6.3. Capacity and SOH estimation

To validate the adaptability and generalization capability of the proposed SOH method, the experiment procedure in Fig. 2 was applied and the battery was placed inside of the chamber. First, the capacity calculation test and charge-discharge process have to be conducted on a fresh battery at different temperatures to make an accurate lookup table reference. Then the cell will be under a cycle/ageing process in a predefined manner. Every 50 cycles, real and estimated SOH are calculated by both the capacity test and the proposed adaptive SOH scheme, respectively. These SOH experiments were conducted at different temperatures of 10 °C, 20 °C, 30 °C, and 40 °C during cycling process as shown in Fig. 15. Moreover, to assess the reliability of the proposed method quantitatively, the SOH estimation errors of the battery at these temperatures and cycles are obtained, as depicted in Fig. 16. As shown, the estimation errors are less than 1.3%, which means that the proposed online SOH estimation method has a good generalization ability in different conditions.

To achieve the desired voltage, power and capacity of an EA/HEA, a battery pack may contain multiple modules consisting of some series and parallel connected cells. The terms *mPnS* and *mSnP* (*m* and *n* are integers) represent two distinct features for a battery

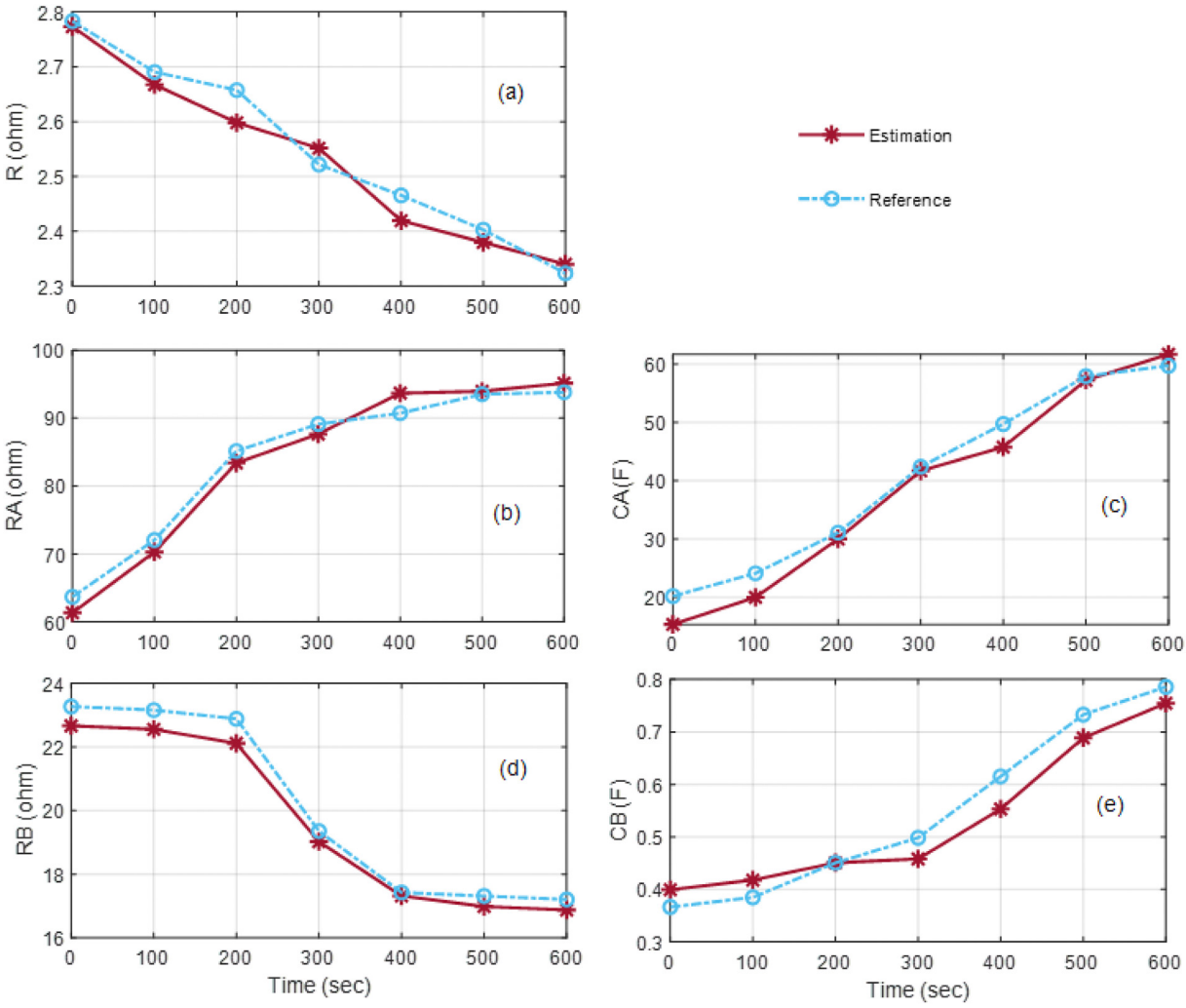

Fig. 10. Cell parameter identification results of the proposed method vs HP PC tests.

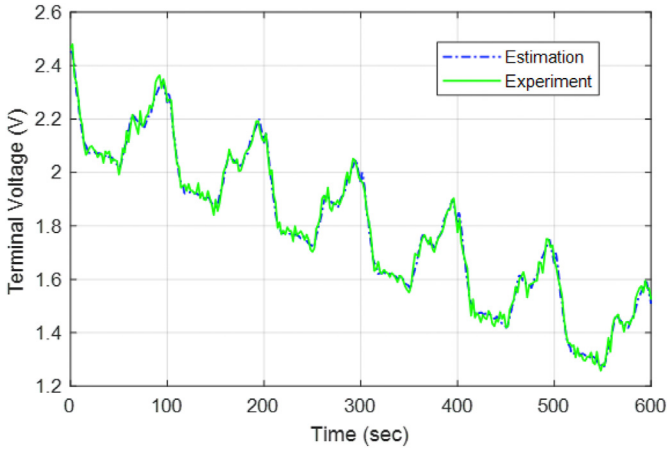

Fig. 11. Battery model validation test.

module. The former term indicates *m* elements in parallel and each has *n* cells in series. And, the second term represents *m* elements in series, each composing of *n* cells in parallel. In this study, nine battery cells in the *3P3S* topology are conected to impement the proposed SOH estimations method at the module level. The battery module contains nine of the same commercial LTO1020 cells that provides the nominal voltage of 7.2 V and capacity of 150 mAh. The cells are fully charged at 1/2 C-rate and until their voltages reach 2.9 V. Then, they are discharged at a constant current of 10 C-rate until their voltage reach the lower cut-off voltage. The conditions of the cells under the experiments are listed in Table 3.

Finally, the proposed online SOH model is validated for nine battery cells at the module level and under the flight cycle shown in Fig. 9. The simulated real-time SOH results (solid lines) of the nine cells are compared to their real SOH values (dash lines) in Fig. 17 (a). As shown, the estimated SOH values are very close to the real SOH values. The test results indicate that the proposed online SOH estimation method is able to predict all cells' SOH within a 1.2% error (Fig. 17). The proposed method is not limited to just the *3P3S* configuration and can be scaled up for HEA/EA application.

7. Conclusion

This study proposed an online SOH estimation method based on an adaptive battery model and adaptive capacity calculation. To develop the proposed method, a combination of an online parameter estimator and an adaptive sliding mode observer has been utilized. Since a high efficent BMS is demanding in electric/hybrid electric aircraft applications, an accurate battery model and online

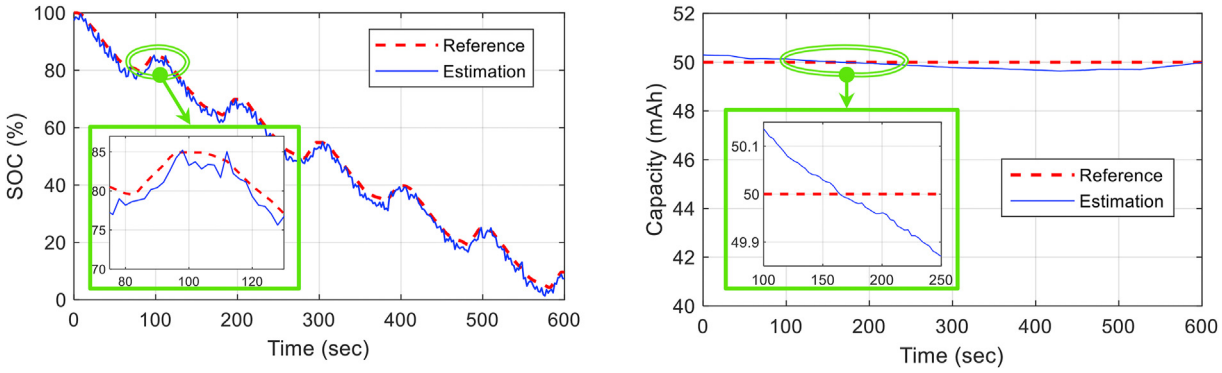

Fig. 12. Adaptive SOC and capacity estimation in high C-rates.

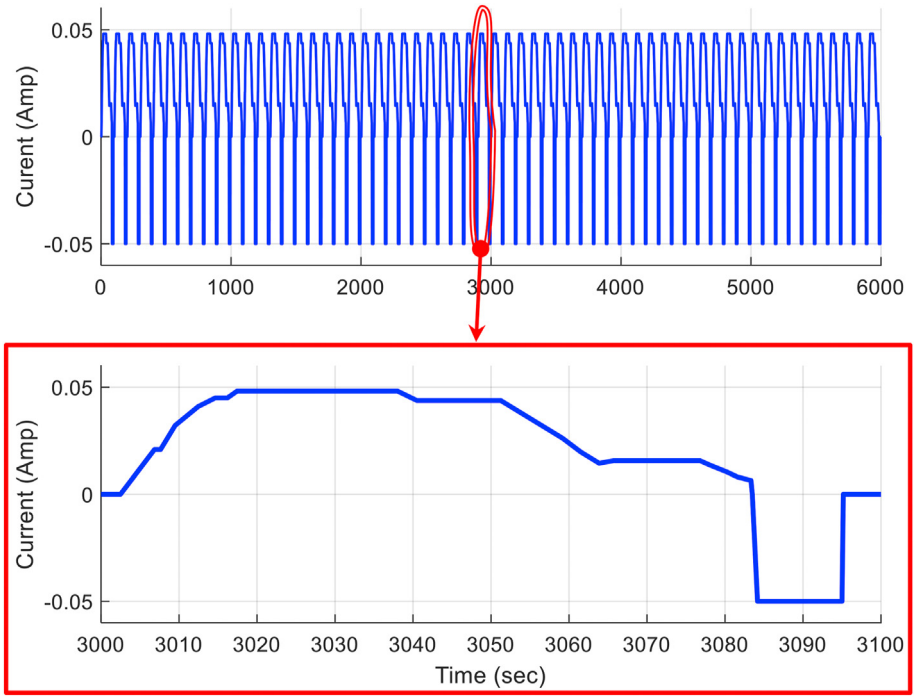

Fig. 13. A sequence of 60 cycles, separated by charge pulses.

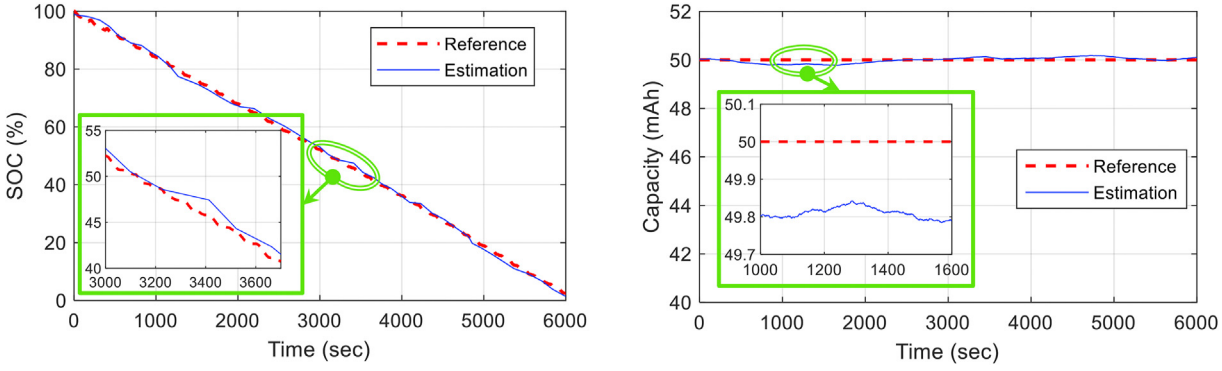

Fig. 14. Adaptive SOC and capacity estimation in low C-rates.

SOH estimation technique for their BMS are developed in this work. At the first stage, an experiment bench for batteries was built by which various tests such as cycling/ageing, HPPC, actual capacity measurment, Coulomb counting, SOC-OCV and flight cycle

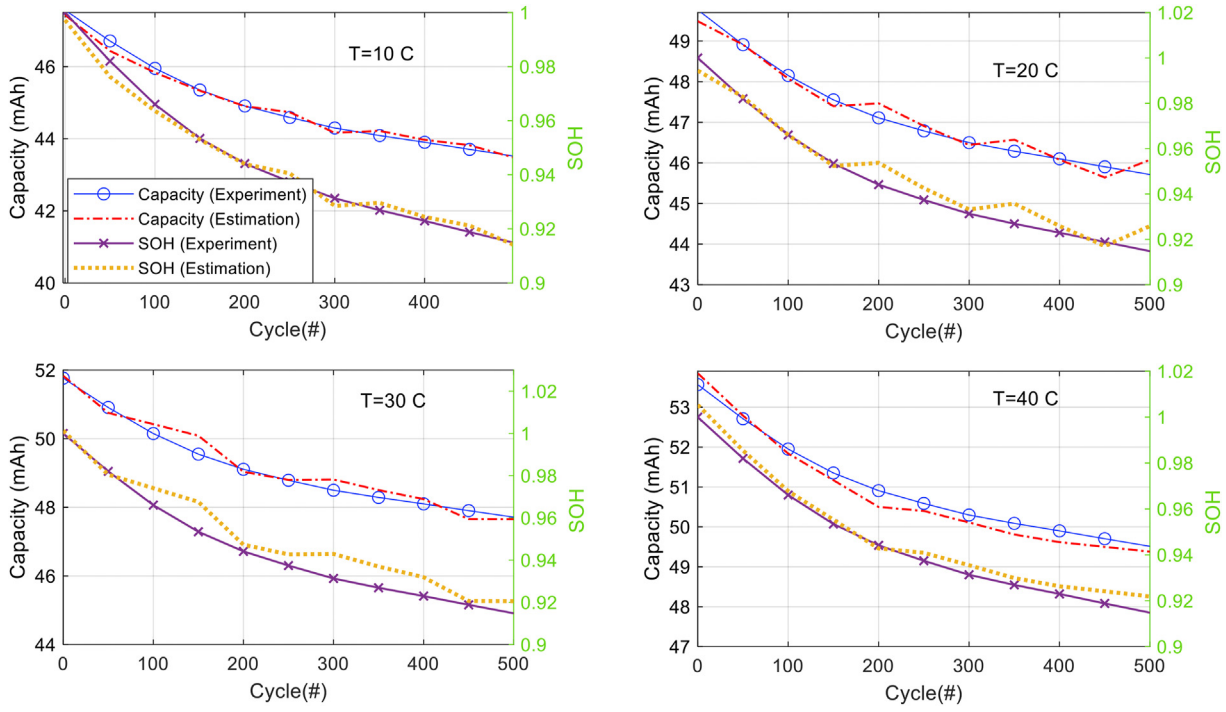

Fig. 15. Online capacity and SOH estimation at different temperatures.

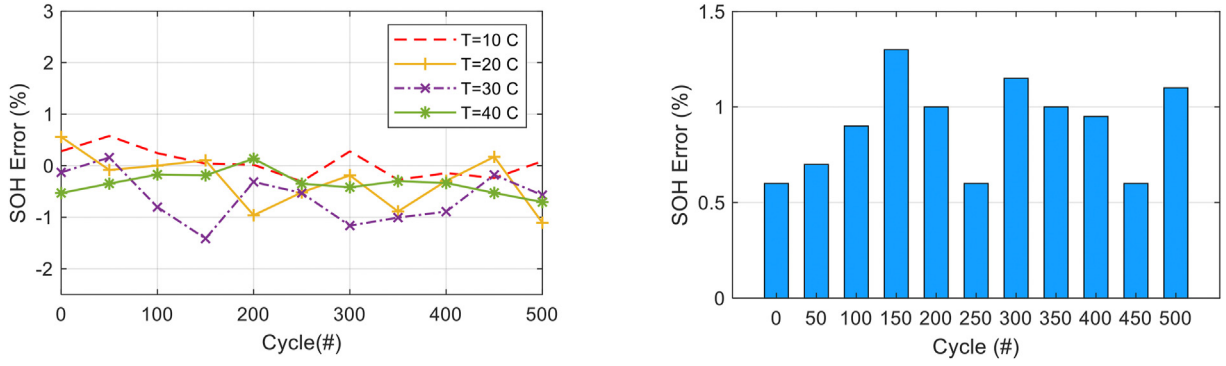

Fig. 16. SOH estimation errors at different temperature conditions.

Table 3
Conditions of the battery cells under online SOH estimation.

Cell #	Expeimental Conditions				
	Upper Cutoff Voltage (V)	Lower Cutoff Voltage (V)	Discharge Current (A)	Temperature (°C)	SOH (%)
1	2.9	1.7	0.5	25	94
2	2.9	1.8	0.5	25	92
3	2.9	1.9	0.5	25	89
4	2.9	1.5	0.5	25	97
5	2.9	1.7	0.5	25	94.2
6	2.9	1.9	0.5	25	88
7	2.9	1.7	0.5	25	93.5
8	2.9	1.6	0.5	25	95
9	2.9	1.9	0.5	25	87.5

validation tests were conducted. Then, a second order battery model was developed to simulate the battery dynamic behavior. In addition, an exponential regression algorithm was exploited to develop the proposed online parameter estimator for the battery model. The experiment results showed the efficiency of the battery model along with the proposed parameter estimator in tracking the dynamic characteristic of the battery. Afterward, an adaptive sliding mode observer and Coulomb counting has been exploited to develop a closed loop SOC estimator. The developed SOC estimator was high accurate in various experiments which make it

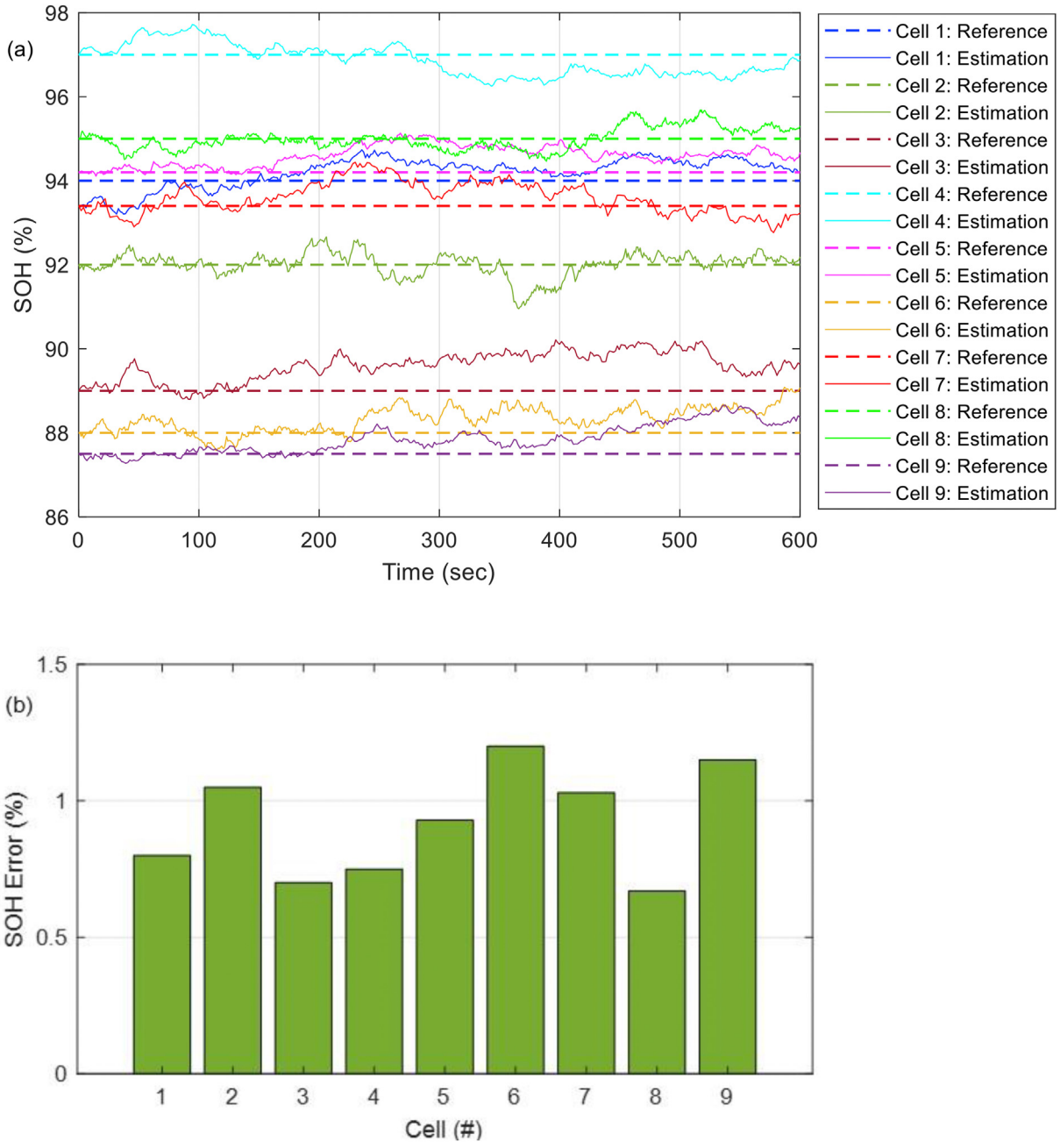

Fig. 17. a) Real-time SOH estimation results compared with the real SOH data at the module level. b) SOH estimation errors are represented by green bars for nine cells. (For interpretation of the references to colour in this figure legend, the reader is referred to the Web version of this article.)

comparable with the results reported previously [26,29]. In the last step, to mitigate the negative impact of operating temperature variation on the accuracy of SOH estimation, an adaptive SOH estimation scheme were developed. To complete the proposed SOH estimation scheme, besides calculating the battery capacity online, we measured the capacity of a fresh battery in different temperature and formed a capacity-temperature lookup table using the experiments. Using various cycling and validation tests and analysis at the cell and module level, the accuracy of the proposed adaptive SOH scheme was tested at the final stage. Based on the experimental results, the error of the proposed SOH scheme was within ±1.3%.

It can be inferred that the proposed online parameter and SOH are suitable for BMS in electric/hybrid electric aircraft applications. Moreover, they can be utilized in both cell and module level to estimate model parameters, SOC and SOH accurately and reliably. In this work, LTO batteries were tested under an ageing process with a constant charging-discharching condition. In future, more tests are needed to explore the proposed method to be applied for different batteries with various chemistries. Moreover, aging process can be conducted with different cycling protocols.

Credit author statement

Seyed Reza Hashemi was the PhD student. He developed the model, did the simulation, got the results, and drafted the manuscript. Dr. Ajay Mohan Mahajan was contributed in advising Mr. Hashemi for model development, simulation and obtaining results.

Dr. Siamak Farhad was contributed in advising Mr. Hashemi for model development, simulation and obtaining results as well as proof reading of the paper.

Declaration of competing interest

The authors declare that they have no known competing financial interests or personal relationships that could have appeared to influence the work reported in this paper.

Acknowledgements

The authors gratefully acknowledge the funding provided by the Ohio Federal Research Network (OFRN) and The University of Akron.

Nomenclature

Symbols and Units Description

I	Battery cell current, A
V_t	Cell terminal voltage, V
R	Ohmic resistance, Ω
C	Capacitance, F
V_A	Voltage over R_1C_1
V_B	Voltage over R_2C_2
H	Coulomb efficiency
C_k	Current capacity of battery
C_n	Nominal capacity of battery cell
k	Time index
t	Time, Sec
T	Temperature, Celsius
J	Sliding mode observer gain
V_{SC}	Switching control vector
T_s	Sample time

Abbreviations

SOC	State of Charge
SOH	State of Health
OCV	Open Circuit Voltage, V
LIB	Lithium-Ion Battery
LTO	Lithium Titanate Oxide
EV	Electric Vehicle
HEV	Hybrid Electric Vehicle
EA	Electric Aircraft
HEA	Hybrid Electric Aircraft
SCT	Standard capacity test
BMS	Battery Management System
HPPC	Hybrid Pulse Power Characterization
EIS	Electrochemical Impedance Spectroscopy
ECM	Equivalent Circuit Model
AECM	Adaptive Equivalent Circuit Model
DP	Dual Polarization
MAPE	Mean Absolute Percentage Error
MAE	Mean Absolute Error
RMSE	Root Mean Square Error

References

[1] Sziroczak D, Jankovics I, Gal I, Rohacs D. Conceptual design of small aircraft with hybrid-electric propulsion systems. Energy 2020;204:117937. Aug 1.
[2] Hoelzen J, Liu Y, Bensmann B, Winnefeld C, Elham A, Friedrichs J, Hanke-Rauschenbach R. Conceptual design of operation strategies for hybrid electric aircraft. Energies 2018;11(1):217. Jan.
[3] Wang S, Zhang S, Ma S. An energy efficiency optimization method for fixed pitch propeller electric aircraft propulsion systems. IEEE Access 2019;7:159986–93. Oct 30.
[4] Bravo GM, Praliyev N, Veress Á. Performance analysis of hybrid electric and distributed propulsion system applied on a light aircraft. Energy 2021;214:118823. Jan 1.
[5] He J, Zhang D, Torrey D. Recent advances of power electronics applications in more electric aircrafts. In: 2018 AIAA/IEEE electric aircraft technologies symposium (EATS). IEEE; 2018. p. 1–8. Jul 12.
[6] Kamal MB, Mendis GJ, Wei J. Intelligent soft computing-based security control for energy management architecture of hybrid emergency power system for more-electric aircrafts. IEEE Journal of Selected Topics in Signal Processing 2018;12(4):806–16. Jun 18.
[7] Liu K, Hu X, Yang Z, Xie Y, Feng S. Lithium-ion battery charging management considering economic costs of electrical energy loss and battery degradation. Energy Convers Manag 2019;195:167–79. Sep. 1.
[8] Ji Z, Rokni MM, Qin J, Zhang S, Dong P. Energy and configuration management strategy for battery/fuel cell/jet engine hybrid propulsion and power systems on aircraft. Energy Convers Manag 2020;225:113393. Dec 1.
[9] Rajalakshmi M, Razia Sultana W. Intelligent hybrid battery management system for electric vehicle. Artificial Intelligent Techniques for Electric and Hybrid Electric Vehicles 2020:179–206. Jul 15.
[10] Tang X, Wang Y, Zou C, Yao K, Xia Y, Gao F. A novel framework for Lithium-ion battery modeling considering uncertainties of temperature and aging. Energy Convers Manag 2019;180:162–70. Jan 15.
[11] Galeotti M, Giammanco C, Cinà L, Cordiner S, Di Carlo A. Synthetic methods for the evaluation of the State of Health (SOH) of nickel-metal hydride (NiMH) batteries. Energy Convers Manag 2015;92:1–9. Mar 1.
[12] Qian K, Huang B, Ran A, He YB, Li B, Kang F. State-of-health (SOH) evaluation on lithium-ion battery by simulating the voltage relaxation curves. Electrochim Acta 2019;303:183–91. Apr 20.
[13] Tian H, Qin P, Li K, Zhao Z. A review of the state of health for lithium-ion batteries: research status and suggestions. J Clean Prod 2020;261:1–30. Mar 13:120813.
[14] Noura N, Boulon L, Jemeï S. A review of battery state of health estimation methods: hybrid electric vehicle challenges. World Electric Vehicle Journal 2020;11(4):66. Dec.
[15] Song S, Fei C, Xia H. Lithium-ion battery SOH estimation based on XGBoost algorithm with accuracy correction. Energies 2020;13(4):812. Jan.
[16] Zheng Y, Qin C, Lai X, Han X, Xie Y. A novel capacity estimation method for lithium-ion batteries using fusion estimation of charging curve sections and discrete Arrhenius aging model. Appl Energy 2019:1–13. Oct 1;251:113327.
[17] Feng X, Weng C, He X, Han X, Lu L, Ren D, Ouyang M. Online state-of-health estimation for Li-ion battery using partial charging segment based on support vector machine. IEEE Trans Veh Technol 2019;68(9):8583–92. Jul 22.
[18] Khumprom P, Yodo N. A data-driven predictive prognostic model for lithium-ion batteries based on a deep learning algorithm. Energies 2019;12(4):660. Jan.
[19] Qu J, Liu F, Ma Y, Fan J. A neural-network-based method for RUL prediction and SOH monitoring of lithium-ion battery. IEEE access 2019;7:87178–91. Jun 27.
[20] Talha M, Asghar F, Kim SH. A neural network-based robust online SOC and SOH estimation for sealed lead–acid batteries in renewable systems. Arabian J Sci Eng 2019;44(3):1869–81. Mar 11.
[21] Murnane M, Ghazel A, et al. A closer look at state of charge (SOC) and state of health (SOH) estimation techniques for batteries. Analog devices 2017;2:426–36. May.
[22] Xiong R, Li L, Tian J. Towards a smarter battery management system: a critical review on battery state of health monitoring methods. J Power Sources 2018;405:18–29. Nov 30.
[23] Xiong R, Tian J, Mu H, Wang C. A systematic model-based degradation behavior recognition and health monitoring method for lithium-ion batteries. Appl Energy 2017;207:372–83. Dec 1.
[24] Li H, Ravey A, N'Diaye A, Djerdir A. Online adaptive equivalent consumption minimization strategy for fuel cell hybrid electric vehicle considering power sources degradation. Energy Convers Manag 2019;192:133–49. Jul 15.
[25] Xu X, Yu C, Tang S, Sun X, Si X, Wu L. State-of-health estimation for lithium-ion batteries based on Wiener process with modeling the relaxation effect. IEEE Access 2019;7:105186–201. Jun 14.
[26] Liu Z, Zhao J, Wang H, Yang C. A New Lithium-Ion Battery SOH Estimation Method Based on an Indirect Enhanced Health Indicator and Support Vector Regression in PHMs. Energies 2020;13(4):830. Jan.
[27] Hashemi SR, Nazari A, Esmaeeli R, Aliniagerdroudbari H, Alhadri M, Zakri W, Mohammed AH, Mahajan A, Farhad S. Fast fault diagnosis of a lithium-ion battery for hybrid electric aircraft. InASME 2018 Power Conference collocated with the ASME 2018. In: 12th international conference on energy sustainability and the ASME 2018 nuclear forum. American Society of Mechanical Engineers Digital Collection; 2018.
[28] Huang H, Wang H, Gu J, Wu Y. High-dimensional model representation-based global sensitivity analysis and the design of a novel thermal management system for lithium-ion batteries. Energy Convers Manag 2019;190:54–72. Jun 15.
[29] Huang SC, Tseng KH, Liang JW, Chang CL, Pecht MG. An online SOC and SOH estimation model for lithium-ion batteries. Energies 2017;10(4):512. Apr.
[30] Rijanto E, Rozaqi L, Nugroho A, Kanarachos S. RLS with optimum multiple adaptive forgetting factors for SoC and SoH estimation of Li-Ion battery. In: In2017 5th international conference on instrumentation, control, and

automation (ICA). IEEE; 2017. p. 73–7. Aug 9.
[31] Hashemi SR, Esmaeeli R, Aliniagerdroudbari H, Alhadri M, Alshammari H, Mahajan A, Farhad S. New intelligent battery management system for drones. In: ASME international mechanical engineering congress and exposition, vol. 59438. American Society of Mechanical Engineers; 2019. Nov 11p. V006T06A028.
[32] Tran MK, Mevawala A, Panchal S, Raahemifar K, Fowler M, Fraser R. Effect of integrating the hysteresis component to the equivalent circuit model of Lithium-ion battery for dynamic and non-dynamic applications. Journal of Energy Storage 2020 Dec 1;32:101785.
[33] Lai X, Wang S, Ma S, Xie J, Zheng Y. Parameter sensitivity analysis and simplification of equivalent circuit model for the state of charge of lithium-ion batteries. Electrochim Acta 2020;330:135239. Jan 10.
[34] Li Y, Vilathgamuwa M, Farrell T, Tran NT, Teague J. A physics-based distributed-parameter equivalent circuit model for lithium-ion batteries. Electrochim Acta 2019;299:451–69. Mar 10.
[35] Frankforter KJ, Tejedor-Tejedor MI, Anderson MA, Jahns TM. Investigation of hybrid battery/ultracapacitor electrode customization for energy storage applications with different energy and power requirements using HPPC cycling. IEEE Trans Ind Appl 2019;56(2):1714–28. Dec 24.
[36] Kollmeyer P, Hackl A, Emadi A. Li-ion battery model performance for automotive drive cycles with current pulse and EIS parameterization. In: 2017 IEEE transportation electrification conference and expo (ITEC). IEEE; 2017. p. 486–92. Jun 22.
[37] Hashemi SR, Bahadoran Baghbadorani A, Esmaeeli R, Mahajan A, Farhad S. Machine learning-based model for lithium-ion batteries in BMS of electric/hybrid electric aircraft. Int J Energy Res 2020;45(4):5747–65. Mar.
[38] Hashemi SR, Esmaeeli R, Nazari A, Aliniagerdroudbari H, Alhadri M, Zakri W, Mohammed AH, Mahajan A, Farhad S. A fast diagnosis methodology for typical faults of a lithium-ion battery in electric and hybrid electric aircraft. Journal of Electrochemical Energy Conversion and Storage 2020;17(1). Feb 1.
[39] Zhou Y, Cao S. Coordinated multi-criteria framework for cycling aging-based battery storage management strategies for positive building–vehicle system with renewable depreciation: life-cycle based techno-economic feasibility study. Energy Convers Manag 2020;226:113473. Dec 15.
[40] Ouyang M, Liu G, Lu L, Li J, Han X. Enhancing the estimation accuracy in low state-of-charge area: A novel onboard battery model through surface state of charge determination. J Power Sources 2014;270(Dec 15):221–37.
[41] Hu Z, Gallacher B. Extended Kalman filtering based parameter estimation and drift compensation for a MEMS rate integrating gyroscope. Sensor Actuator Phys 2016;250:96–105. Oct 15.
[42] Lee SD, Jung S. An adaptive control technique for motion synchronization by on-line estimation of a recursive least square method. Int J Contr Autom Syst 2018;16(3):1103–11. Jun 1.
[43] Islam SA, Bernstein DS. Recursive least squares for real-time implementation [lecture notes]. IEEE Contr Syst Mag 2019;39(3):82–5. May 16.
[44] Wen S, Qi H, Ren YT, Sun JP, Ruan LM. Solution of inverse radiation-conduction problems using a Kalman filter coupled with the recursive least–square estimator. Int J Heat Mass Tran 2017;111:582–92. Aug 1.
[45] Xia Q, Xu A, Du L, Yan Y, Wu S. High-rate, long-term performance of LTO-pillared silicon/carbon composites for lithium-ion batteries anode under high temperature. J Alloys Compd 2019;800:50–7. Sep. 5.
[46] Jiang C, Wang S, Wu B, Fernandez C, Xiong X, Coffie-Ken J. A state-of-charge estimation method of the power lithium-ion battery in complex conditions based on adaptive square root extended Kalman filter. Energy 2021;219:119603. Mar 15.
[47] Kalogiannis T, Hosen MS, Sokkeh MA, Goutam S, Jaguemont J, Jin L, Qiao G, Berecibar M, Van Mierlo J. Comparative study on parameter identification methods for dual-polarization lithium-ion equivalent circuit model. Energies 2019;12(21):4031. Jan.
[48] Ouyang T, Xu P, Chen J, Lu J, Chen N. Improved parameters identification and state of charge estimation for lithium-ion battery with real-time optimal forgetting factor. Electrochim Acta 2020;353. Jun 11:136576.
[49] Li J, Wang L, Lyu C, Liu E, Xing Y, Pecht M. A parameter estimation method for a simplified electrochemical model for Li-ion batteries. Electrochim Acta 2018;275:50–8. Jun 10.
[50] He J, Feng D, Hu C, Wei Z, Yan F. Two-layer online state-of-charge estimation of lithium-ion battery with current sensor bias correction. Int J Energy Res 2019 Jun 25;43(8):3837–52.
[51] Liu Y, Liao YG, Lai MC. Development and validation of a lithium-ion polymer battery cell model for 12V SLI battery applications. In: International design engineering technical conferences and computers and information in engineering conference, vol. 51784. American Society of Mechanical Engineers; 2018. Aug 26p. V003T01A038.
[52] Tian J, Xiong R, Yu Q. Fractional-order model-based incremental capacity analysis for degradation state recognition of lithium-ion batteries. IEEE Trans Ind Electron 2018;66(2):1576–84. Jan 26.
[53] Kim T, Qiao W, Qu L. Online SOC and SOH estimation for multicell lithium-ion batteries based on an adaptive hybrid battery model and sliding-mode observer. In: 2013 IEEE energy conversion congress and exposition. IEEE; 2013. p. 292–8. Sep. 15.